

# Assessment of particle characterisation via phase Doppler anemometry and automated particle image analysis techniques

J. T. Kashdan<sup>1</sup>, J. S. Shrimpton<sup>1</sup>, H. J. Booth<sup>2</sup> and A. Whybrew<sup>2</sup>

<sup>1</sup>Department of Mechanical Engineering, Imperial College of Science, Technology & Medicine, London, UK.

<sup>2</sup>Imaging Division, Oxford Lasers Ltd, Abingdon, Oxfordshire, UK. Sizing@oxfordlasers.com

## ABSTRACT

A comparison between two droplet sizing techniques has been made. Phase Doppler (PDA) anemometry and particle / droplet imaging analysis (PDIA) have been applied to a hollow cone fuel spray under quasi-steady conditions. Measurements of the arithmetic mean ( $D_{10}$ ) and volume mean ( $D_{30}$ ) diameters were made at three locations in the spray. The first location referred to as the ‘atomisation’ region at  $Z=5\text{mm}$  from the nozzle exit was found to consist of large coherent and mostly non-spherical liquid masses or ligaments (Fig. 1(a)). Although images revealed the presence of a small number of droplets in this region, their high velocities (up to  $40\text{m/s}$ ) caused significant motion blur and thus the PDIA method was unable to make measurements. At  $Z=10\text{mm}$  (Fig. 1 (b)) and without applying any shape constraints to the PDIA data, a comparison of volume mean diameters showed good agreement for the spatial volume mean ( $D_{30}$ ) estimates between the PDIA ( $D_{30}=30.9\mu\text{m}$ ) and PDA ( $D_{30}=32.5\mu\text{m}$ ). Applying progressively more stringent shape constraints with PDIA had the effect of reducing  $D_{10}$  and  $D_{30}$  as only the smaller (and therefore more spherical) droplets were sized. In the ‘dispersed spray’ region at  $Z=20\text{mm}$ , the majority of the liquid mass was in the form of spherical droplets with a significantly lower droplet concentration (Fig. 1(c)). At this location, without applying a DOF correction, a comparison of the PDIA ( $D_{30}=25.0\mu\text{m}$ ) and PDA ( $D_{30}=24.3\mu\text{m}$ ) data again showed good agreement. It was observed that the effect of a depth of field (DOF) correction, which accounts for the fact that smaller droplets are less likely to be in focus biases the pdf’s by adding smaller droplets such that the  $D_{10}$  and  $D_{30}$  estimates were significantly reduced. Such deviations were probably due to the DOF calibration which was limited to a minimum  $D=16\mu\text{m}$ .

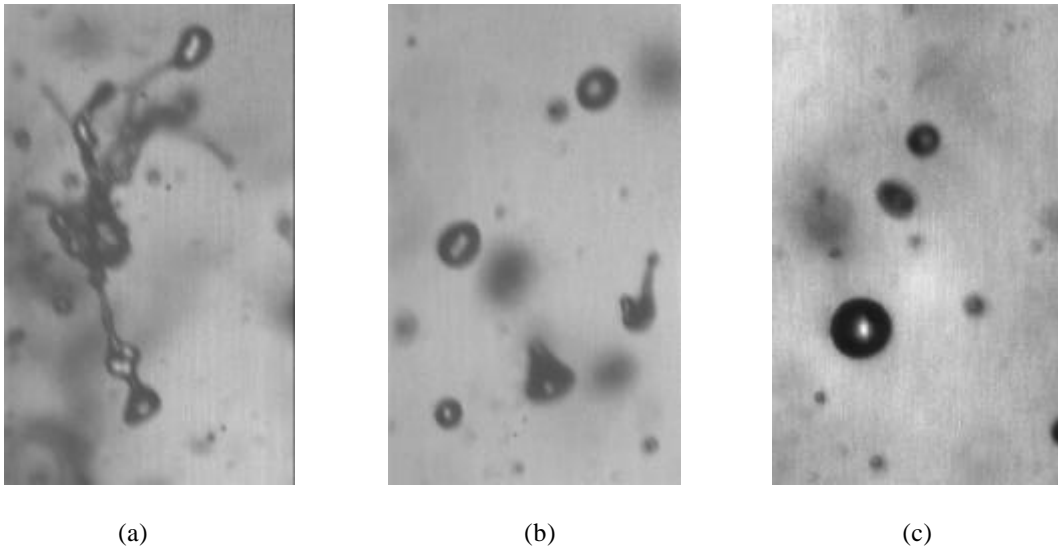


Fig. 1 Spray images at axial locations of (a)  $Z=5\text{mm}$ , (b)  $Z=10\text{mm}$  and (c)  $Z=20\text{mm}$  corresponding to ‘atomisation’, ‘dense spray’ and ‘dispersed spray’ regions.

The first results from this investigation confirm that the PDIA method can accurately size droplets of  $D>15\mu\text{m}$  in moderately dense sprays however it is evident that to analyse sprays of smaller characteristic scales, the calibration is vital for producing more accurate number distributions. PDA measurements at  $Z=5\text{mm}$  were possible however the PDIA images at this location suggested the presence of very few spherical drops and although it was possible to gather data using PDA under these conditions, one must treat the data measured with a degree of uncertainty.

## 1. INTRODUCTION

In a remarkable range of industrial applications, knowledge and control of multiphase flow phenomena is vital for predictive and profitable process operation. For instance in powder manufacturing and food production processes the continual monitoring of droplet size distribution is often necessary to establish some form of quality control (Crowe et al, 1998). Multiphase flows are generally complex systems with sprays/plumes commonly consisting of droplets which have a range of properties. This property range almost always includes droplet diameter, velocity and concentration, usually includes non-sphericity, mass/heat transfer and temperature variations. In addition, other properties that are commonly present in some regions of the spray/plume include droplet break-up, physical property variations and coalescence. At the most basic level multiphase flows may be characterised by an average spray length scale, however there are a number of definitions and this is a source of much confusion. Standard texts (Lefebvre, 1989; Bayvel & Orzechowski, 1993) give definitions and the two most commonly used are  $D_{10}$  and  $D_{32}$ . The linear average diameter ( $D_{10}$ ) is defined as the diameter of a uniform drop set with the same number and sum of diameters as the real set, providing a simple 'average' measure with which to compare different sprays. However, most multiphase processes involve heat and/or mass transfer and the representative length scale used here is the Sauter mean diameter ( $D_{32}$ ) which is the diameter of a uniform drop set with the same total volume and total surface area as the real set. For steady-state combustion systems (Brandt et al, 1998), stability and emissions are drastically affected by the quality of atomisation and also the distribution of drop diameter, velocity and concentration within the spray. The experimental challenges are further increased when transience or periodicity in the flow is present. Directly injected fuel sprays in diesel (Coghe & Cossali, 1994; Wigley & Pitcher, 1997) and more recently gasoline engines (Wigley et al, 1998; Le Coz, 1998, Arcoumanis et al, 1999) are a classic example and problems are exacerbated by the hostile measurement conditions and poor optical access. In addition obtaining statistically accurate data is problematic in the developing spray region because it is generally harder to quantify the larger length scales due to ill-defined shape and their (numerical) scarcity. Computational multiphase prediction methods (Gosman & Clerides, 1998, Beck and Watkins, 1999) are continually improving but are hindered by two mutually exclusive problems. The first is that liquid atomisation at industrially relevant conditions although extensively visualised (Engelbert et al, 1995; Abo-Serie et al, 1999) lacks any analytical foundation and the semi-empirical sub-models that do exist are still strongly based on empiricism and suffer from a plethora of tuneable constants. The second is that accurate estimates of the initial drop sizes in the primary break-up region are difficult to obtain since the majority of droplet measurement techniques available work most efficiently in dispersed regions where most droplets are spherical. Such information is needed for example, as input boundary conditions in CFD spray models which require user-defined initial drop diameter and velocities. The current approach is to inject characteristic 'parcels' of liquid and rely on empirical sub-models and their tuneable constants to produce sensible solutions (Ahmadi-Befrai et al, 1979; Habchi et al, 1997; Arcoumanis et al, 1999; Beale & Reitz, 1999).

In the present work the objective is to evaluate the relative merits of two drop-sizing methods. The first method is phase Doppler anemometry (PDA) which is generally considered to be an accurate method for spray characterisation. The second method, referred to as particle/droplet image analysis (PDIA) is based on the automated analysis of digital images of the spray, which are processed to give drop-size data. This work not only considers the accuracy of each method in estimating drop size distributions but also the ease and time required for calibration and set-up, the measurement time required to obtain statistically accurate datasets and finally complexities and assumptions associated with data / image post-processing.

## 2. OVERVIEW OF MEASUREMENT METHODS

A wide range of optically based droplet size measurement techniques have been developed which generally fall into one of two categories; direct imaging (Azzopardi, 1979) or light scattering (Lading et al, 1994). The most important sub-class being single drop counting methods and Black et al (1996) provides an extensive review. Other methods include ensemble light scattering methods of droplet sizing that integrate in one dimension (Swithenbank, 1976) and more recently planar methods (Yeh et al, 1993; Domann & Hardalupas, 2000). Phase Doppler anemometry (Durst et al, 1976; Bachalo et al, 1984) is generally considered the most accurate method for spray characterisation despite its high capital cost and the requirement for skilled operation in order to optimise the system set-up and subsequent data interpretation. The technique relies on measuring the time delay that occurs when the light scattered by a droplet traversing the intersection of two coherent laser beams arrives at two spatially separated photo detectors. Through good design and proper set-up the method has the potential to gather accurate data at extremely high data rates with good statistical certainty. However measurement accuracy is dependent on a number of factors including laser power, optical configuration, droplet homogeneity, sphericity and concentration and requires skilled set-up and operation to obtain good results. One of the fundamental limitations of PDA is the inability to accurately measure non-spherical droplets (Damaschke et al, 1997). Such conditions are observed at the interface where an initial liquid sheet breaks up into ligaments subsequently forming initially large and often non-spherical droplets, therefore PDA is an inherently unsuitable instrument to characterise near-orifice flows. This is an unfortunate limitation, since the

near-orifice region is where the spray is defined and the process of atomisation is occurring. This creates particular problems for data certainty, since only a small fraction of the spray mass is spherical. In addition the best optical geometry is specific (Pitcher & Wigley, 1992, 1994) and may not be available in the experiment and curved window surfaces need complex optical corrections to be employed which while valid for LDA work (Stieglmeier et al, 1989) are difficult to extend to PDA. An alternative and more direct method to determine information on droplet sizes is image analysis. The major advantage is that a visual record of the spray under investigation provides a simple means to check what is and (more importantly) is not being measured and the ability to quantify arbitrarily shaped objects. Until recently the error and time required for manual analysis of the images (Bayvel & Orzechowski, 1993) has been the reason why direct imaging methods have not been more prevalent. However the ongoing development of low cost, high resolution and semi-automated imaging apparatus has removed these difficulties and the method deserves re-evaluation.

## 2.1 PDIA Instrumentation

Oxford Lasers 'VisiSizer' Solo software provided an automated PDIA method (Whybrew et al, 1999) to obtain average diameter information from a set of 8 bit shadow images of a spray. The imaging investigation made use of a non-intensified 12-bit CCD camera (PCO Sencam) offering a resolution of 1280x1024 pixels and a minimum exposure time of 100ns whilst illumination was provided by a diffuse beam from a diode laser (Whybrew et al, 1999) operated in single shot mode. A long distance microscope lens (Infinity K2) with a focal length of 51mm gave a nominal magnification factor of  $M=8.9$  with a resolution of  $0.755\mu\text{m}/\text{pixel}$  from the CCD pixel dimension of  $6.7\mu\text{m}$ . The camera and laser were arranged in line such that back illuminated images were obtained. A thresholding algorithm was then applied to the images in order to distinguish between droplets which appear as dark objects against the illuminated background. Droplet diameters and equivalent droplet diameters for non-spherical drops were then measured based on the pixel area of the droplets. The absolute minimum measurable length scale is ultimately limited by diffraction effects and is approximately  $1\mu\text{m}$  however the software limit requires at least five pixels to obtain a measurement. With the present hardware the minimum measurable length scale was approximately  $3\mu\text{m}$  and is comparable to the absolute limits of the PDA technique using standard equipment. The upper measurement range is a function of the magnification employed and is completely hardware dependent i.e. there is no theoretical upper limit. A software limit exists such that the largest droplets should be no more 25% of the CCD sensor. For a typical  $1\text{k} \times 1\text{k}$  camera, this corresponds to a maximum diameter of 250 pixels providing a dynamic size range of 50:1. This dynamic range is easily extendable by using bigger chips in contrast with PDA, where a 40:1 dynamic range is fundamentally limited by the non linear scattered light intensity - diameter relationship.

In order to produce unbiased distributions with the PDIA method care must be taken to consider the properties of the droplets as they move in and out of focus. Obviously the droplet image is sharpest for droplets lying in the plane of the focus of the optical system, sometimes referred to as the plane of best focus (Fig. 2) and there is a finite distance in front of and behind this plane in which droplets will still appear to be 'in focus'. This distance is known as the depth of field (DOF) and is determined by the lens to subject distance and lens focal length ( $f$ ).

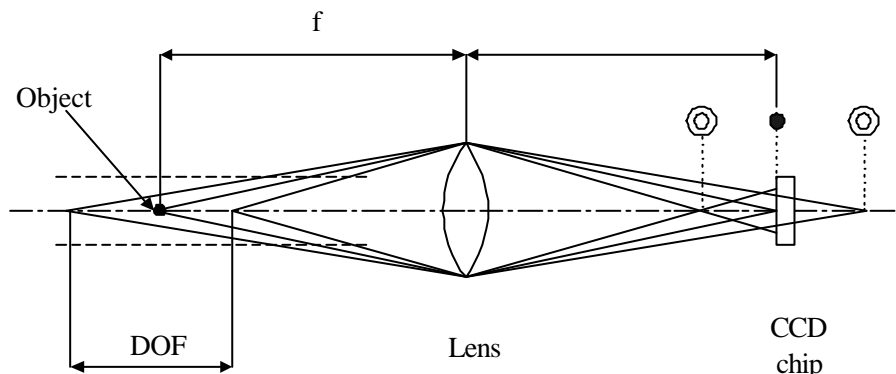


Fig. 2 The effect of droplet position within the depth of field (DOF) on image focus

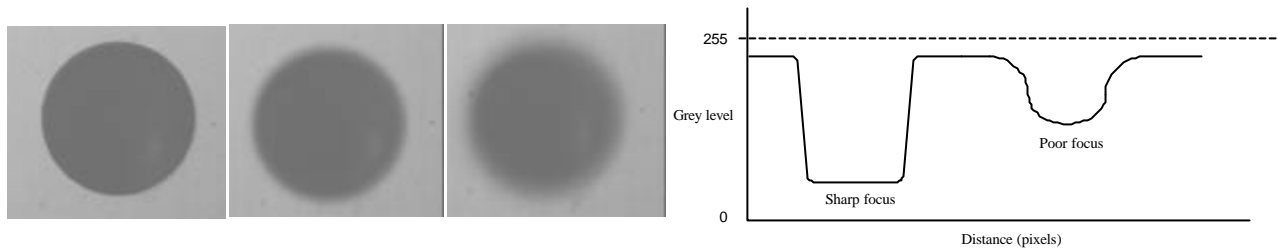


Fig. 3 Calibration images showing effect of object position and grey scale gradient dependence with plane of focus

As a droplet is moved away from the plane of best focus the sharpness of its image degrades (Fig. 3) and produces an increasingly blurred ‘halo’ around the outer periphery (Chigier, 1991). Depth of field is a function of droplet diameter, thus the three-dimensional interrogation area or measurement volume varies with droplet diameter in a manner analogous to PDA measurement volume variation. Providing the optical characteristics of the image system are known a correction may be applied to the obtained droplet diameter probability density function again in a similar manner to PDA. Jones (1976) and Yule et al (1978) addressed the problems associated with determining focus that removed the human eye from the process and were able to quantify this parameter in terms of apparent area and edge gradient. This allowed estimates of the displacement from the plane of focus and true diameter to be obtained. An apparent area,  $A_T$  is calculated from the number of pixels in the image of a droplet which are darker than a background threshold value. Between the dark uniform interior and the thresholded background, there exists a ‘halo’ of grey levels that range from the dark interior to the background level. This ‘halo’ is described by its area,  $A_H$ , its perimeter,  $P$  and its gradient,  $G$ .  $G$  is the grey level gradient which varies across the inner and outer regions of the halo and is thus independent of the actual grey levels present. There exists a unique relationship between  $A_T$ ,  $A_H$  and  $D$  with translation from the plane of focus. This DOF calibration requires calibration for a given hardware set up and in the present work was accomplished by translation (with an accuracy of  $\pm 1\mu\text{m}$ ) of a glass slide etched with black discs (Fig. 3) with sizes ranging from  $16\mu\text{m}$  to over  $300\mu\text{m}$ . Figure 4 shows for this hardware configuration how the apparent area varies as (a) a function of true area and (b) translation from the plane of focus.

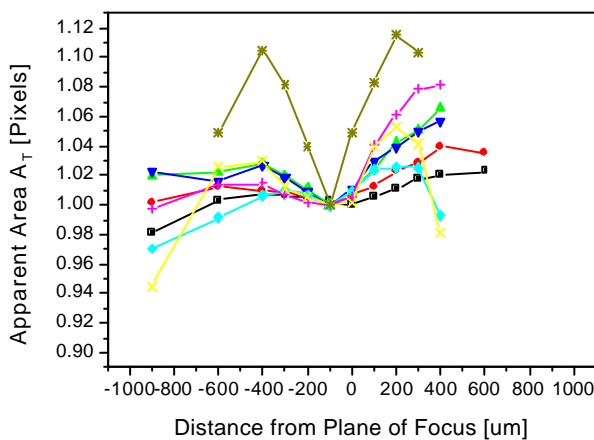


Fig. 4 Calibration graph showing variation of apparent area as a function of distance from focus plane.

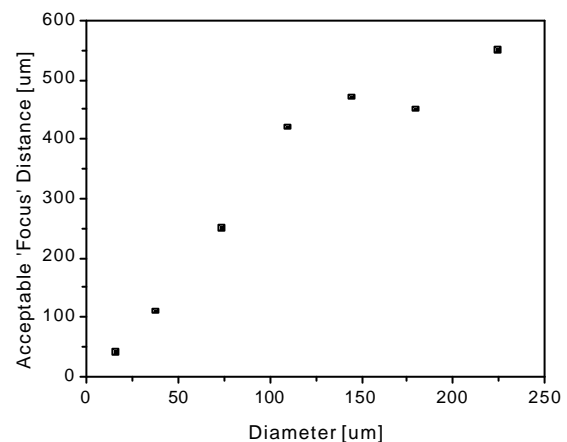


Fig. 5 Graph showing effect of  $D$  on interrogation volume.

The maximum distance, where the droplet merges into the background is greater for larger drops thus implying that the interrogation volume is a function of droplet diameter (Fig. 5). Also there is a maximum translation for each object beyond which the apparent diameter may be multi-valued. This condition is avoided by considering the halo area ( $A_H$ ) which varies as shown in Fig. 6 for the same conditions as shown in Fig. 4.

A proprietary algorithm is used to set these maximum distances for each size class. Obviously this should be less than the multi-valued condition and in the present work the acceptable distance was defined as 70% of the translation giving maximum object area. Since the depth of field and therefore the interrogation volumes vary with droplet size class, a correction should be made to the number and volume distributions obtained. The use of this correction is explored below.

## 2.2. PDA Instrumentation

The PDA system employed was a hybrid Dantec/Aerometrics system. A Dantec 55X transmission system was employed and this incorporated a Bragg cell to shift one beam by 40MHz and was configured to the specifications given in table 1. By employing beam expansion of the green line of a nominal 3W argon ion laser a fringe spacing of  $3.02\mu\text{m}$  was obtained and a measurement volume diameter of approximately  $81.2\mu\text{m}$ . Light collection was made at a  $30^\circ$  off axis condition where signal quality was found to be superior to that at the preferred Brewster condition. The problem of poor signals at the Brewster condition was found to be due to noise from two sources, firstly low light intensity/excessive photomultiplier voltage and also a noisy Bragg cell driver signal. Using lenses of focal lengths of 310mm for the transmission unit and 500mm for the Aerometrics (RCV100) receiving optics gave a phase factor of  $0.713^\circ/\mu\text{m}$ . Predictions of the phase linearity using STREU showed that linearity was good for  $D > 10\mu\text{m}$ , below this maximum errors of upto 16% are predicted. The Aerometrics receiver possesses a third detector with a resolution half this to give a maximum drop size of approximately  $90\mu\text{m}$  and given that the dynamic range of the photomultipliers is around 1:40 this gives a minimum drop diameter of approximately  $2\mu\text{m}$  which is comparable with the PDIA method. Using an Aerometrics processor (RSA3100-P) the raw signals were sent firstly through a high pass filter (20MHz) and then amplified thus increasing the signal amplitude but compressing the overall dynamic range of amplitudes. The log-amp signal was then sent through a low pass filter (40MHz) to remove high frequency noise and signal visibility of approximately 70% was obtained. The 'sphericity check' validation of the Aerometrics software which compares diameters based on the fine ( $\phi_{12}$ ) and range ( $\phi_{13}$ ) phase angles was ignored in the present set of experiments as were the intensity validation checks which nominally remove large slow drops and small fast ones. The far field measurement conditions were near-ideal in terms of signal quality and rate and errors in the diameter and velocity means are thought to be near the minimum for the measurement technique and the results depend more on the resolution of the data interrogation area and the method used for surface data representation than the points themselves.

## 3. EXPERIMENTAL SET-UP

The aim of the work presented is to assess the performance of PDIA and PDA in real sprays and the example chosen is from the authors current research, a fuel spray (Fig. 7) from a pressure swirl atomiser designed for direct injection gasoline engines. The fuel injection system and global characteristics such as spray angle and penetration rate have been obtained (Arcoumanis et al, 1999) and form the basis for the current work. Conical sprays were chosen because drop concentration varies inversely as the cube of the distance from the orifice which gives rise to rapid changes in spray character with increasing axial distance from the nozzle exit. Data acquisition was triggered by a programmable PC timer card (Amplicon PC212E) which also triggered either the PDIA or PDA hardware, as shown in Fig. 8. Previous work (Arcoumanis et al, 1999) has shown that for  $t_{aSOI} > 0.3\text{ms}$  the spray cone is in a quasi steady state and measurements were made at  $t = 1.8\text{ms}$  aSOI for the PDIA method whilst an acquisition window of 1.7 to 1.9ms aSOI was used for the PDA measurements. An injection pressure of 10bar was chosen to minimise image blur since the time period for acquisition was limited by the minimum exposure time ( $0.1\mu\text{s}$ ) rather than the laser pulse width. This low pressure, while not representative of fuel injection in no way lessens the general applicability of the

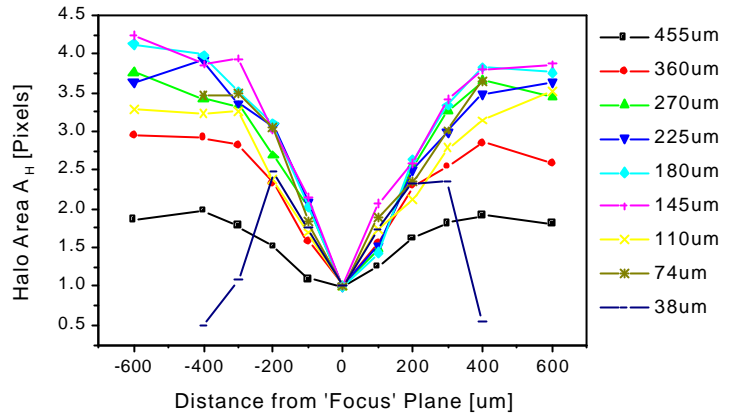


Fig. 6 Calibration graph showing variation of halo area with distance from focus plane

Table 1 PDA system characteristics

| Optical Parameters            | Transmitting Optics | Units          |
|-------------------------------|---------------------|----------------|
| Laser wavelength              | 514.5               | nm             |
| Laser power at mv             | $38.6 \times 10^6$  | $\text{W/m}^2$ |
| Beam diameter at focus lens   | 2.5                 | mm             |
| Beam separation at focus lens | 54                  | mm             |
| Focusing lens focal length    | 310                 | mm             |
| Fringe spacing                | 3.02                | $\mu\text{m}$  |
| Measurement volume diameter   | 81                  | $\mu\text{m}$  |
|                               | Receiving Optics    |                |
| Scattering angle              | 30                  | $^\circ$       |
| Collection lens focal length  | 500                 | mm             |
| Slit width                    | 50                  | $\mu\text{m}$  |
| Diameter range                | 2 to 88             | $\mu\text{m}$  |
| Velocity range                | -61 to 110          | m/s            |

work and higher pressures (and faster sprays) could easily be investigated providing faster (but more expensive) hardware was available.



Fig. 7 Typical spray image at  $t=1.8\text{ms aSOI}$ ,  $P_{inj}=20\text{bar}$ .

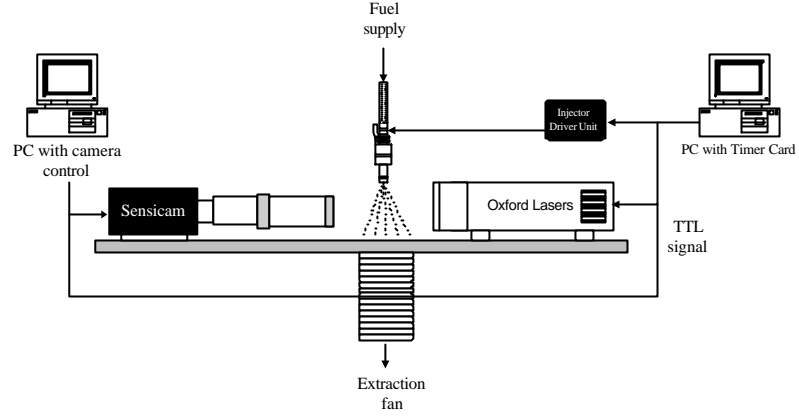


Fig. 8 Schematic diagram showing experimental arrangement for the PDIA technique

### 3.1 Data Interpretation and Errors

Since data from two dissimilar measurement techniques is compared a discussion of the format of the derived results and their relationship is required. A comparison of ‘average’ diameter measurements is made and this quantity has a number of definitions as previously mentioned. Number ( $D_{10}$ ) and volume ( $D_{30}$ ) means are investigated since comparisons will reveal the sensitivity between the methods to measuring small and large drops respectively.  $D_{10}$  and  $D_{30}$  defined in equation (1), represent the most accurate measurements possible since a population of  $N$  drops are individually considered.

$$D_{ab} = \left( \frac{\sum_{n=1}^N D_n^a}{\sum_{n=1}^N D_n^b} \right)^{1/a-b} \quad \text{where} \quad D_{10} = \frac{\sum_{n=1}^N D_n}{N}, \quad D_{30} = \left( \frac{\sum_{n=1}^N D_n^3}{N} \right)^{1/3} \quad (1)$$

An alternative method to obtain these average quantities is, from the probability density function (pdf) of drop diameter,  $n(D)$ , and volume,  $v(D)$ ,

$$\int_{D_{\min}}^{D_{\max}} n(D)dD = 1, \quad \int_{D_{\min}}^{D_{\max}} V(D)dD = 1 \quad (2)$$

derive a finite difference approximation,

$$D_{ab} = \left( \frac{\sum_{i=1}^I n_i D_i^a}{\sum_{i=1}^I n_i D_i^b} \right)^{1/a-b} \quad \text{where} \quad D_{10} = \frac{\sum_{i=1}^I n_i D_i}{\sum_{i=1}^I n_i}, \quad D_{30} = \left( \frac{\sum_{i=1}^I n_i D_i^3}{\sum_{i=1}^I n_i} \right)^{1/3} \quad (3)$$

where in this case  $D_i$  is the midpoint and  $n_i$  the drop population of the  $i$ th size class. PDIA interrogates space instantaneously whereas PDA considers the spray flux through an elemental area for a given time. Equations (1) to (3) apply to the PDIA and PDA techniques separately, but to compare data between the two techniques we must remove the residence time bias of the spatial distribution. This may be done by making use of the joint pdf of diameter and velocity  $n(D,U)$  or volume and diameter,  $n(V,U)$ . This is a simple process since we measure  $U_z$  and  $D$  simultaneously with the PDA technique, thus to convert the temporally based PDA data to the spatially based form for direct comparison to the PDIA technique we must apply the following transformation to size classes,

$$n(D_i)_{\text{spatial}} = \frac{\bar{U}}{\bar{U}_i} n(D_i)_{\text{temporal}}, \quad V(D_i)_{\text{spatial}} = \frac{\bar{U}}{\bar{U}_i} V(D_i)_{\text{temporal}} \quad (4)$$

where  $\bar{U}$  is the average velocity of all samples and  $\bar{U}_i$  is the mean of the  $i$ th size class. This procedure is a source of error since we are assuming a mean velocity for a size class whereas in fact the spread about the mean may be

considerable. Care must also be taken to attempt to compare like with like. For example it has been shown above how the interrogation region for PDIA is larger for bigger droplets and the same behaviour is found in laser anemometry (Saffman, 1987; Hardalupas & Taylor, 1989). A correction should be made to the number and volume pdfs for biasing pdfs in PDIA since larger droplets are more likely to be in contact with the edge of the interrogation region (which has dimensions  $H \times W$ ) than their smaller cousins. For the VisiSizer software this is defined as

$$\frac{1}{1-n_i} = \frac{WH}{(W-D_i)(H-D_i)} \quad (5)$$

Again similar edge effects occur in PDA, however these are much more difficult to quantify. Lastly we have factors that are spray dependent and are most suitable for investigation in this comparative study. In particular we discuss how the PDIA and the PDA perform in absolute measurement terms, i.e. accuracy of a single pdf measurement and how system performance degrades with increasing harshness of the measurement conditions. In the present study this is confined to variation of drop concentration and the presence of non-spherical liquid masses.

#### 4. RESULTS

Preliminary photographs of the spray under investigation have shown the presence of three distinct regions and these have been termed ‘atomisation’, ‘dense spray’ and ‘dispersed spray’. These locations were at axial ( $Z$ ) displacements of 5, 10 and 20mm from the nozzle exit. Figure 1 shows the nature of the spray in these regions. The near nozzle ‘atomisation’ region reveals the presence of large liquid masses in the form of irregular and mostly non-spherical volumes (ligaments) where only a few small number of spherical droplets existed. At  $Z=10$ mm, the ‘dense spray’ region showed that a large number of discrete droplets had formed although a few non-spherical liquid masses remained. At an axial distance of  $Z=20$ mm the vast majority of the liquid was in the form of spherical droplets with a significantly lower drop concentration. The mean axial and rms velocities, obtained from PDA at the three locations as a function of time aSOI are shown (Fig. 9) confirming that at  $t \approx 1.8$ ms, quasi-steady conditions

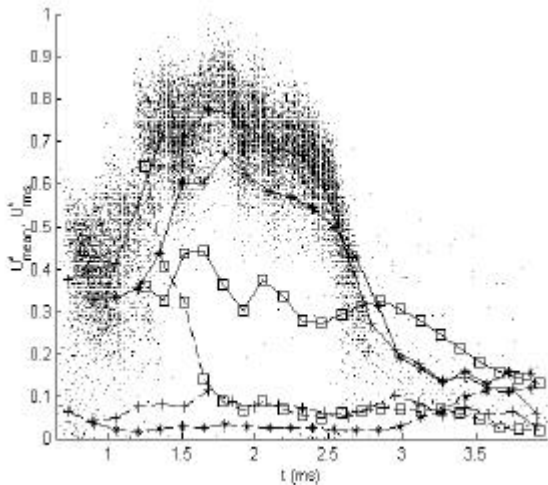


Fig. 9 PDA Data,  $U_{mean}$  (solid) and  $U_{rms}$  (dashed) profiles for  $0 < t < 4$ ms where  $+ = 5$ mm,  $* = 10$ mm and  $\square = 20$ mm downstream.  $U_{norm} = 50$ m/s. Overlaid scatter plot from  $z = 5$ mm data

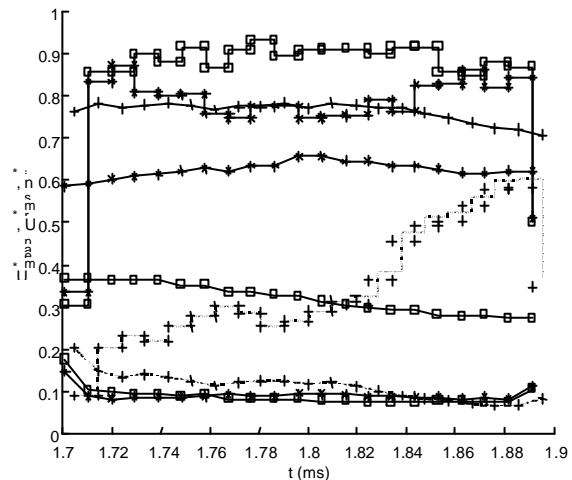


Fig. 10 PDA Data,  $U_{mean}$  (solid) and  $U_{rms}$  (dashed) and sample number (dotted) profiles for  $1.7 < t < 1.9$ ms where  $+ = 5$ mm,  $* = 10$ mm and  $\square = 20$ mm downstream.  $U_{norm} = 50$ m/s,  $N_{norm} = 1700$

exist at each interrogation region. Figure 9 also shows periodic velocity fluctuations which have previously been observed (Wigley et al, 1998; Nouri et al, 1999) with such pressure swirl atomisers. The main spray lasts until about 2.7ms aSOI after which the velocities fall to zero. It is noted that at  $Z=10$  and 20mm the discrete sample plots reveal a much broader range of velocities for  $1.5 < t < 2.8$ ms than for the 5mm location. Note that although the  $U_{rms}$  profiles are similar the  $U_{mean}$  reduces from  $Z=5$ mm to  $Z=20$ mm whilst the relative turbulence intensities increase markedly away from the injector. The quasi-steady assertion is confirmed by considering Fig. 10 which shows that 12000, 28000 and 31000 valid samples were gathered using PDA for the  $Z=5$ , 10 and 20mm locations respectively. Figure 10 also shows that average and rms velocity for each interrogation region varied by approximately 5% over the time interval and samples were relatively evenly acquired over the time duration. This gives confidence to the quasi-steady assertion made above and permits comparison between instantaneous methods such as PDIA. In the following subsections a comparison of the PDA and PDIA results is made for the three interrogation regions,  $Z=5$ ,

10 and 20mm. In the following text the superscripts ‘T’ and ‘S’ denote the temporal and spatial forms of the distributions.

#### 4.1 PDA and PDIA : data comparison for Z=20mm

At Z=20mm the measurement conditions are benign, with large inter-drop separations and a low probability of non-spherical liquid masses. These conditions permitted a useful comparison of the accuracy of the two methods. As shown in table 2 there is a close correlation between the two sets of results where the PDA (Fig. 11) and PDIA valid sample counts were 30,790 and 5,411 respectively. The first four rows of table 2 show how various corrections and transformations affect the average diameters from data obtained with the PDA system. Condition (a) shows the results for  $D_{10}$  and  $D_{30}$  for all drops considered individually and condition (b) shows the numerical change in converting these quantities to

Table 2 PDA and PDIA integrated diameter results for Z=20mm

| Source | Conditions  | $D_{10}$ ( $\mu\text{m}$ ) | $D_{30}$ ( $\mu\text{m}$ ) |
|--------|---|----------------------------|----------------------------|
| PDA    | (a) eqn(1) – no probe vol correction              | 21.8 <sup>T</sup>          | 26.5 <sup>T</sup>          |
| PDA    | (b) eqn(1) + eqn (4)                              | 19.4 <sup>S</sup>          | 24.3 <sup>S</sup>          |
| PDA    | (c) eqn(3) – no probe vol correction              | 23.0 <sup>T</sup>          | 28.3 <sup>T</sup>          |
| PDA    | (d) eqn(3) - probe vol correction (Saffman, 1987) | 21.9 <sup>T</sup>          | 26.0 <sup>T</sup>          |
| PDIA   | (e) No corrections                                | 15.2 <sup>S</sup>          | 25.0 <sup>S</sup>          |
| PDIA   | (f) Edge correction (eqn. 5)                      | 15.7 <sup>S</sup>          | 25.7 <sup>S</sup>          |
| PDIA   | (g) DOF correction                                | 8.5 <sup>S</sup>           | 15.2 <sup>S</sup>          |
| PDIA   | (h) DOF and edge corrections                      | 8.7 <sup>S</sup>           | 15.6 <sup>S</sup>          |

spatial quantities to allow direct comparison with the PDIA technique. Conditions (c) and (d) calculated  $D_{10}$  and  $D_{30}$  using weighted midpoints, e.g. eqn (3) with the Aerometrics PDA software (Dataview) and are included to show the magnitude of the effect of a probe volume correction algorithm (Saffman, 1987) on the results. As shown the effect is to reduce  $D_{10}$  and  $D_{30}$  by  $1\mu\text{m}$  and  $2\mu\text{m}$  respectively. The authors are surprised at the magnitude of the difference between conditions (a) and (c) which sampled 30000 and 11000 samples respectively. The software for condition (a) was written in house and has been tested against analytical test cases giving accuracy significantly better than is implied by table 2 and the error is ascribed to the finite difference approximation of equation (3) in condition (c). Applying the magnitude of the probe volume correction shown by comparing conditions (c) and (d) to the spatial  $D_{10}$  and

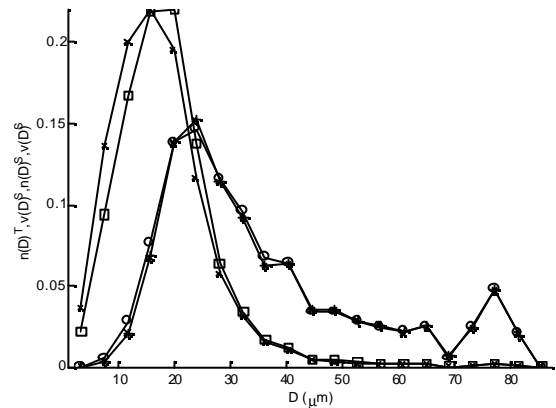


Fig. 11 PDA data, number and volume pdfs for Z=20mm,  $1.7 < t < 1.9\text{ms}$  where  $\bullet = n(D)^T$ ,  $\ast = V(D)^T$ ,  $+ = n(D)^S$ ,  $\circ = V(D)^S$

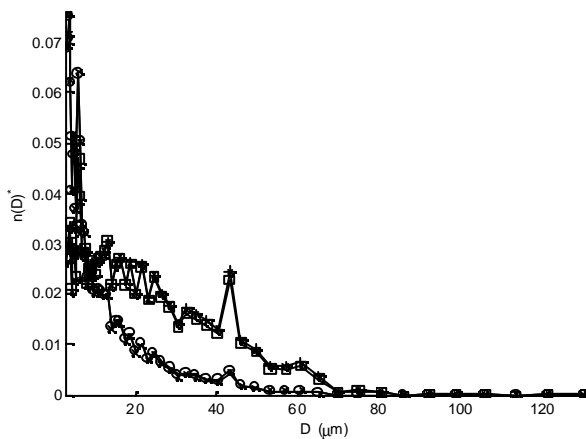


Fig. 12 PDIA Data at Z=20mm showing effect of DOF & edge correction on number distribution where  $\bullet$  (no correction),  $\ast$  (edge only),  $\times$  (DOF only) and  $\circ$  (DOF and edge correction)

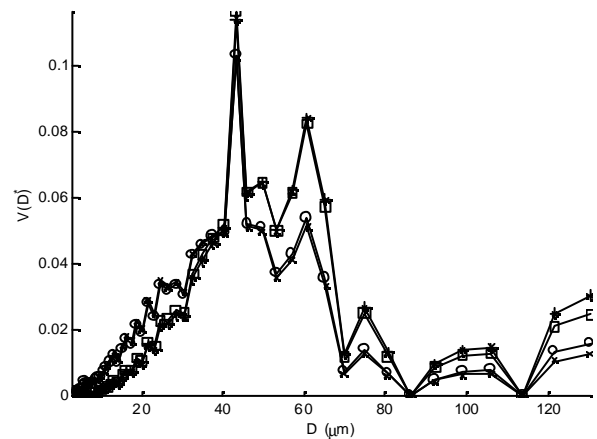


Fig. 13 PDIA data at Z=20mm showing effect of DOF & edge correction on volume distribution where  $\bullet$  (no correction),  $\ast$  (edge only),  $\times$  (DOF only) and  $\circ$  (DOF and edge correction)

$D_{30}$  (condition b) we see that the effective probe volume corrected spatially averaged  $D_{10}$  and  $D_{30}$  from the PDA data at  $Z=20\text{mm}$  are 18 and  $22\mu\text{m}$  to a probable accuracy of  $1\mu\text{m}$ . Comparing this with the PDIA results (Figs. 12 & 13) shows that there is a high degree of correlation for the  $D_{30}$  results and this confirms that the PDIA and the PDA method can accurately size drops of  $15\mu\text{m}$  upwards. Applying the edge correction algorithm (eqn 5) to the raw pdfs (condition (e)) gives the result shown in condition (f), table 2. The small correction is entirely sensible considering the large interrogation area in relation to the small characteristic scales to be measured. In actual fact the PDA results are underestimating the characteristic lengths because the maximum diameter limit is  $88\mu\text{m}$  and PDIA technique confirmed that drops in excess of  $100\mu\text{m}$  exist at this location and time. The PDIA technique is known to measure single large (of the order  $100\mu\text{m}$ ) drops from sprays with a high degree of accuracy (Wigley et al 2000). The DOF correction, which preferentially biases the smaller drop classes of the number and volume distributions seems to produce unusual results. A number of reasons could be responsible. Firstly, the calibration relies on test objects translated about the plane of focus to obtain the result shown in Fig. 5 and the shape of the object should be the same as the objects being analysed. While the shapes were representative, the minimum calibration length was not at the lower end of the size range, being at  $16\mu\text{m}$ , thus some deviation would be expected to occur below this limit. The DOF correction algorithm, which essentially operates on the calibration curve to correct for small drops having smaller measurement volumes than larger ones will greatly amplify any calibration errors at small characteristic lengths if not properly bounded. To summarise this section, and considering conditions (b) and (f) and taking into account of a probe volume correction to the PDA data of  $1\mu\text{m}$  for  $D_{10}$  and  $2\mu\text{m}$  for  $D_{30}$  respectively agreement is good. The fact that both  $D_{10}$  and  $D_{30}$  agree to within 1 or  $2\mu\text{m}$ , which are sensitive to opposite ends of the distribution gives a high level of confidence in both methods. One proviso is that in these initial results the PDA data has not been processed to remove the fastest drops of the distribution. Strictly this is necessary to compare like with like since the PDIA will have a more restrictive maximum velocity limit, dictated by motion blur. For the relaxed focus criteria used in the present work with the PDIA method the effect of motion blur will be to size droplets slightly smaller than their actual size. In the following subsection sphericity issues are investigated for the  $Z=10\text{mm}$  location where droplet concentration is higher.

#### 4.2 PDA and PDIA : data comparison for $Z=10\text{mm}$

At  $Z=10\text{mm}$  the inter-drop distances are reduced and there exists a more dense spray. We now take a standard set up for further comparison for both methods. For PDA this is condition (b) from table 2 with a proviso that a probe volume correction will reduce the spatial averages by 1- $2\mu\text{m}$ . For PDIA this

Table 3 PDA and PDIA integrated diameter results for  $Z=10\text{mm}$

| Source | Conditions  | $D_{10}$ ( $\mu\text{m}$ ) | $D_{30}$ ( $\mu\text{m}$ ) |
|--------|---|----------------------------|----------------------------|
| PDA    | (a) eqn(1) – no probe vol correction              | 27.9 <sup>T</sup>          | 34.0 <sup>T</sup>          |
| PDA    | (b) eqn(1) + eqn (4)                              | 26.4 <sup>S</sup>          | 32.5 <sup>S</sup>          |
| PDIA   | (c) Edge correction (eqn. 5), no sphericity check | 18.9 <sup>S</sup>          | 30.9 <sup>S</sup>          |
| PDIA   | (d) Edge correction, reject $S<0.3$               | 12.7 <sup>S</sup>          | 22.5 <sup>S</sup>          |
| PDIA   | (e) Edge correction, reject $S<0.5$               | 11.2 <sup>S</sup>          | 19.7 <sup>S</sup>          |
| PDIA   | (f) Edge correction, reject $S<0.8$               | 3.8 <sup>S</sup>           | 4.2 <sup>S</sup>           |

means employing edge correction whilst neglecting the DOF correction which tended to produce unusual results which is probably due to poor calibration. Neglecting the DOF correction will effectively produce pdfs with proportionally larger dropsizes because of the larger measurement volume. However this particular subsection, using a standard set up for PDA and PDIA investigates the effect of varying the sphericity parameter on the PDIA results which ultimately may be useful in interpreting PDA data (Fig. 14). Although there does exist the capacity to assess ‘sphericity’ via PDA this is done over two closely spaced points on the drop surface. This measure cannot assess shape and thus the analysis is confined to true ‘sphericity’ based on image interrogation. Without applying any sphericity constraints a comparison of the PDA number and particularly volume pdfs at  $Z=10\text{mm}$  and  $20\text{mm}$  revealed that the small drops were still being measured and that the peak of the number pdf

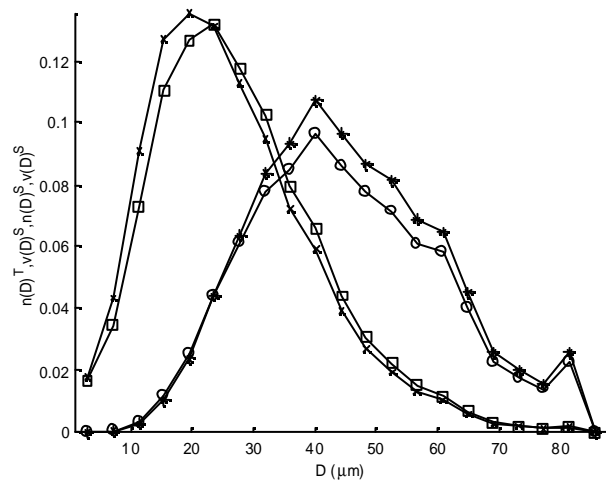


Fig. 14 PDA Data, number and volume pdfs for  $Z=10\text{mm}$ ,  $1.7 < t < 1.9\text{ms}$  where  $\bullet = n(D)^T$ ,  $* = V(D)^T$ ,  $+ = n(D)^S$ ,  $o = V(D)^S$

still occurs at approximately  $20\mu\text{m}$ . However the breadth of the distributions are much wider at  $Z=10\text{mm}$  and in this case causes the volume mean in particular to shift to a higher value. The cause of this is at first unclear although strongly spherical objects are present at  $10\text{mm}$ , their relative frequency is not any higher than at  $20\text{mm}$ . From an examination of the images however it is clear that non-sphericity is the norm and that most of the droplets of a size that affect the volume are oscillating in all directions. The PDA counts these droplets and sizes them incorrectly because the instrument is only sampling over a small fraction of the surface. Unfortunately, as has been discussed previously this is not confined to 1-D PDA systems, since standard 2-D and 3-D systems also only recover phase information from one component. The opposite trend in average diameter is found comparing the PDIA results for the  $Z=10\text{mm}$  and  $Z=20\text{mm}$  interrogation zones, again by examining tables 2 and 3 where the average diameters decrease.

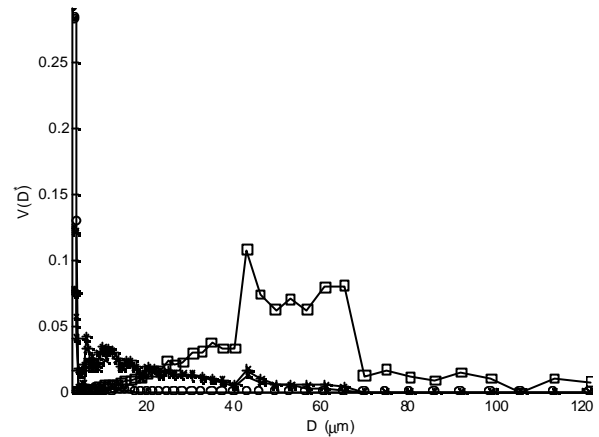
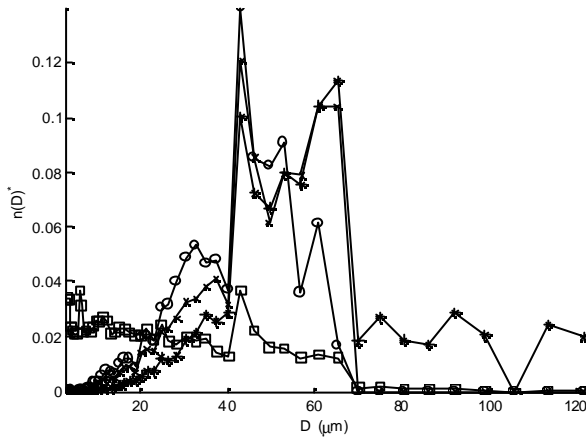


Fig. 15 PDIA Data at  $Z=10\text{mm}$  showing effect of shape factor variation on number distribution where  $\bullet$  (no shape validation),  $*$  ( $S=0.3$ ),  $\times$  ( $S=0.5$ ) and  $\circ$  ( $S=0.8$ )

Fig. 16 PDIA Data at  $Z=10\text{mm}$  showing effect of shape factor variation on volume distribution where  $\bullet$  (no shape validation),  $*$  ( $S=0.3$ ),  $\times$  ( $S=0.5$ ) and  $\circ$  ( $S=0.8$ )

Note that the DOF correction is not being applied at  $Z=10\text{mm}$  and the number and volume pdfs shown in Figs 15 and 16 are uncorrected. We further checked a random selection of images to ensure that these drops (a) do actually exist (b) exist in sufficient numbers and (c) were being sized to acceptable accuracy and both these conditions were found to hold. Thus it would appear that the PDIA generated pdfs are representative and the PDA data suffers from three shortcomings. Firstly the larger drops are not being counted as  $D_{\text{max}}$  is greater than  $88\mu\text{m}$ , secondly that many small drops are not being counted, making the number pdf of the PDA misleading and thirdly the drop oscillations are artificially broadening both the number and the volume pdfs. This last point may be investigated quantitatively further by re-processing the PDIA data and operating on the sphericity parameter  $S$ . By making  $S$  progressively more severe we can filter out the non-spherical objects from the distribution and examine the remainder. By setting  $S$  to 0.3, 0.5 and 0.8 we remove 53%, 69% and 85% of the samples respectively and clearly from the  $D_{10}$  and  $D_{30}$  trends, progressively smaller diameters are considered. The fact that 53% of the distribution is lost for a shape factor,  $S < 0.3$  does suggest that a large fraction of the measurable objects are non-spherical, which violates one of the key PDA assumptions. We now consider the most severe, near nozzle measurement condition at  $Z=5\text{mm}$ .

### 4.3 PDA and PDIA : Comparison for $Z=5\text{mm}$

At  $Z=5\text{mm}$  we obtained data from the PDA instrumentation (Fig. 17) and this has already been shown in Figs. 9 and 10. From Fig. 10 we see that the samples are skewed towards the end of the  $1.7 < t < 1.9\text{ms}$  time window which suggests that data is easier to obtain at the end of the period. Also, from Fig. 10, the mean velocity is approximately  $40\text{m/s}$  and the rms velocity is small. This implies that all the liquid is travelling at approximately the same speed. Images of this region (e.g. Fig. 1) revealed large coherent structures, at various orientations to the field of view. Obviously sizing these structures assuming sphericity would not produce any useful information and subsequent analysis of these images with the PDIA algorithm showed that the only measurements recorded were of very small drops in the range  $4 < D < 6\mu\text{m}$ . It was reassuring that no erroneously large drops were recorded and this suggests a certain robustness of the algorithm. An examination of the images revealed that a mixture of small drops and parts of the ligaments were recorded as measurable droplets, particularly those structures that passed through the focal plane in the image. It is clear that the PDIA technique cannot measure accurately in such conditions for several reasons. Firstly the structures are not spherical and they are sufficiently irregular to produce anomalies that are statistically significant. Secondly and most importantly the high concentration of objects in the field of view and its uneven

distribution makes thresholding an individual image difficult and almost impossible to fix a threshold for a set of images due to the large variations in background average grey level intensity. Lastly the majority of the liquid is simply moving too fast to freeze the image. It is clearly an advantage of the PDA to be able to measure in such harsh conditions and the success of the technique has been proven under more severe conditions than demonstrated in the present investigation. However the images at this position suggested the presence of very few spherical drops and although it may be possible to gather data using PDA under these conditions, one must treat the data with some degree of scepticism.

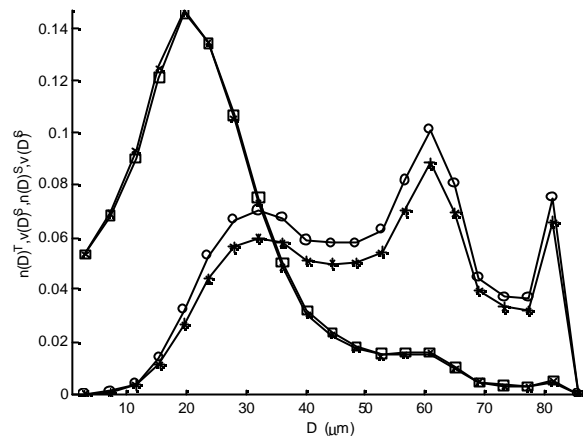


Fig. 17 PDA Data, number and volume pdfs for  $Z=5\text{mm}$ ,  $1.7 < t < 1.9\text{ms}$  where  $\bullet = n(D)^T$ ,  $* = V(D)^T$ ,  $+ = n(D)^S$ ,  $o = V(D)^S$

## SUMMARY

Two droplet sizing techniques, PDA and PDIA have been applied to a quasi-steady hollow cone fuel spray. A comparison of the results in moderately dense spray conditions at  $Z=10$  and  $20\text{mm}$  showed good agreement for  $D_{30}$ . In addition, the effects of depth of field and sphericity corrections have been examined for the PDIA method at these locations. Applying the PDIA method in the near nozzle region ( $Z=5\text{mm}$ ) did not yield accurate data and images revealed the presence of ligament structures whilst most droplets present were inaccurately sized due to excessive image blur.

## ACKNOWLEDGEMENTS

The authors would like to thank Dr J. Nouri of Imperial College for helpful advice concerning the PDA set-up, E. Abo-Serie and F. Hall for assistance with the test rig and EPSRC (GR/M17969) for financial support.

## REFERENCES

- Abo-Serie, E., Arcoumanis, C., Gavaises, M., Argueyrolles, B., Galzin, F., (1999) "Structure of Sprays generated by Pressure-Swirl Injectors for Direct Injection Gasoline Engines", Proc. ILASS-Europe'99, Toulouse 5-7, July, 1999.
- Ahmadi-Befrai, B., Gosman, A. D., Issa, R. I., Watkins, A. P., (1990) "EPISO, An Implicit non-iterative Solution procedure for the Calculation of Flows in Reciprocating Engine Chambers", Comp. Methods in Appl. Methods & Eng., 79, pp. 249-279, 1990.
- Arcoumanis, C., Gavaises, M., French, B., (1997) "Effect of Fuel Injection Processes on the Structure of Diesel Sprays", SAE Paper 970799, 1997.
- Arcoumanis, C., Gavaises, M., Argueyrolles, B., Galzin, F., (1999) "Modeling of Pressure-Swirl Atomisers for GDI Engines", SAE Paper 1999-01-0500, 1999.
- Arcoumanis, C., Kashdan, J. T., Shrimpton, J. S., Gaade, J. E., Wallace, S., (1999) "Spray Characteristics of Swirl Pressure Atomisers for Direct-Injection Gasoline Engines", Proc. MechE conf., S492/S1/99, London, December 1999.
- Azzopardi, B. J., (1979) "Measurement of Drop Sizes", Int. J. Heat & Mass Transfer, vol. 22, pp. 1245-1279, 1979.
- Bachalo, W. D., Houser, M. J., "Development of the Phase/Doppler Spray Analyser for Liquid Drop Size and Velocity Characterisations", 20<sup>th</sup> Joint Propulsion Conf., AIAA, Ohio, June, 1984.
- Bayvel, L., Orzechowski, Z., (1993) "Liquid Atomization", Taylor & Francis Publ., ISBN 0-89116-959-8, 1993.
- Beale, J. C., Reitz, R. D., (1999) "Modeling Spray Atomisation with the Kelvin-Helmholtz / Rayleigh-Taylor Hybrid Model", Atomisation & Sprays, vol. 9, pp. 623-650, 1999.

- Beck, J. C., Watkins, A. P., (1999) "Spray Modelling Using the Moments of the Droplet Size Distribution", Proc. ILASS-Europe'99, Toulouse, July 5-7, 1999.
- Black, D. L., McQuay, M. Q., Bonin, M. P., (1996) "Laser-Based Techniques for Particle Size Measurement: A Review of Sizing Methods and their Industrial Applications", Prog. Energy Comb. Sci., vol. 22, pp. 267-306, 1996.
- Brandt, M., Rachner, M., Schmitz, G., (1998) "An Experimental and Numerical Study of Kerosine Spray Evaporation in a Premix Duct for Gas Turbine Combustors at High Pressure", Comb. Sci. & Tech., Vol. 138, pp. 313-348, 1998.
- Chigier, N. A., (1991) "Optical Imaging of Sprays", Prog. Energy & Comb. Sci., vol. 17, no. 3, 1991.
- Coghe, A., Cossali, G. E., (1994) "Phase Doppler Characterisation of a Diesel Spray Injected into a High Density Gas under Vaporisation Regimes", Proc. 7<sup>th</sup> Int. Symp. Appl. Laser Tech. To Fluid Mech., Paper 36.3, Lisbon, 1994.
- Crowe, C., Sommerfield, M., Tsuji, Y., (1998) "Multiphase Flows with Droplets & Particles", CRC Press.
- Damaschke, N., Gouesbet, G., Grehan, G., Mignon, H., Tropea, C., (1997) "Response of PDA Systems to Non-Spherical Droplets", Proc. ILASS-Europe, pp. 382-388, Florence, Italy, 1997.
- Domann, R., Hardalupas, Y., (2000) "Evaluation of the Planar Drop Sizing Technique", ICLASS 2000, California, 2000.
- Durst, F., Zare, M., (1975) "Laser Doppler Measurements in Two Phase Flows", Proc. LDA-Symp., pp. 403-429, Copenhagen, 1975.
- Engelbert, C., Hardalupas, Y., Whitelaw, J. H., (1995) "Breakup Phenomena in Coaxial Airblast Atomisers", Proc. R. Soc. Lond., pp. 189-229, 1995.
- Gosman, A. D., Clerides, D., (1998) "Diesel Spray Modeling: A Review", Invited Lecture, Proc. ILASS-1998, Florence, Italy, July 9-11, 1998.
- Habchi, C., Verhoeven, D., Huu, C. H., Lambert, L., Vanhemelryck, J. L., Baritaud, T., (1997) "Modeling Atomisation and Break Up in High-Pressure Diesel Sprays", SAE Paper, 970881, 1997.
- Hardalupas, Y., Taylor, A. M. K. P., (1989) "On the measurement of particle concentration near a stagnation point", Experiments in Fluids, vol 8, pp. 113-118.
- Jones, A. R., (1977) "A Review of Drop Size Measurement – The Application of Techniques to Dense Fuel Sprays", Prog. Energy Combust. Sci., 3, pp. 225-234, 1977.
- Lading, L., Wigley, G., Buchave, P., (1994) "Optical Diagnostics for Flow Processes", pp. 175-228, Plenum Press, 1994.
- Le Coz, J. F., (1998) "Comparison of Different Drop Sizing Techniques on Direct Injection Gasoline Sprays", 9<sup>th</sup> Int. Symp. Appl. Laser Tech. Fluid Mech., Paper 7.3, 1998.
- Lefebvre, A. H., (1989) "Atomization and Sprays", Hemisphere Publ. Corp., New York, ISBN 0-89116-603-3, 1989.
- Pitcher, G., Wigley, G., (1992) "A Study of the Break-up and Atomisation of a Combusting Diesel Spray by Phase Doppler Anemometry", Proc. 6<sup>th</sup> Int. Symp. Appl. Laser Tech. Fluid Mech., Lisbon, 1992.
- Pitcher, G., Wigley, G., (1994) "Simultaneous Two-component Velocity and Drop-size Measurements in a Combusting Diesel Spray", Proc. 7<sup>th</sup> Int. Symp. Appl. Laser Tech. Fluid Mech., Lisbon, 1994.
- Saffman, M., (1987) "Automatic Calibration of LDA measurement volume size, Applied optics, 26, 13, pp. 2592-2597.
- Stieglmeier, M., Tropea, C., Weiser, N., Nitsche, W., (1989) "Experimental Investigation of the Flow through Axisymmetric Expansions", Trans. ASME, J. Fluids Eng., vol. 111, pp. 464-471, 1989.

Swithenbank, J., Beer, J. M., Taylor, D. S., Abbot, D., McCreath, C. G., (1976) "A Laser Diagnostic for the Measurement of Droplet and Particle Size Distribution", AIAA Paper, no. 76-99, Jan. 1976.

Whybrew, A., Nicholls, T. R., Boaler, J. J., Booth, H. J., (1999) "Diode Lasers – A Cost Effective Tool for Simultaneous Visualisation, Sizing and Velocity Measurements of Sprays", Proc. ILASS-Europe, Toulouse, July 5-7, 1999.

Wigley, G., Heath, J., Whybrew A., (2000) "Experimental analysis of the response of a PDA system to a polydisperse GDI spray" to be presented at the 10<sup>th</sup> Int. Symposium on Applications of Laser Anemometry to Fluid Mechanics.

Wigley, G., Pitcher, G., (1997) "The Effect of Fuel Line Pressure and Injection Duration on Diesel Spray Formation and Structure", Proc. ILASS-Europe, 1997.

Wigley, G., Hargrave, G. K., Heath, J., (1998) "A High Power, High Resolution LDA/PDA System Applied to Dense Gasoline Direct Injection Sprays", 9<sup>th</sup> Int. Symp. On Appl. Laser Tech. To Fluid Mech., Paper 9.4, Lisbon, 1998.

Yule, A. J., Chigier, N. A., Cox, N. W., (1978) "Measurement of Particle Sizes in Sprays by the Automated Analysis of Spark Photographs", Particle Size Analysis, pp. 61-73, Heyden Press, 1978.